LOCAL FIELDS IN CAVITY SITES OF ROUGH DIELECTRIC SURFACES ☆

Naomi LIVER, Abraham NITZAN
Department of Chemistry, Tel Aviv University, Tel Aviv 69978, Israel

and

J.I. GERSTEN
Department of Physics, City College of the City University of New York, New York, New York 10031, USA

Received 26 June 1984

The results of recent experiments which indicate that surface-enhanced Raman scattering from molecules adsorbed on coldly evaporated silver films is associated with cavity sites is interpreted as an electromagnetic field enhancement in regions enclosed by several silver grains. No such enhancement is obtained for a wedge geometry. Cavity sites are seen to be also strong enhancement centers for resonance optical phenomena such as fluorescence and photochemical yield.

1. Introduction

The role of electromagnetic effects in surface-enhanced Raman scattering (SERS) and other surface-enhanced electromagnetic processes is now well established [1]. It is also generally believed that these electromagnetic effects cannot account for all the observations made on SERS and that some (1–2 orders of magnitude) of the observed enhancement may be due to chemical effects (i.e. electronic interactions between the substrate and adsorbate) like those suggested by the adatom model [2]. Recent SERS experiments on coldly deposited silver films [3,4] indicate that molecules which give the stronges SERS signal are located not on top of protrusions or within large scale grating structures (which are the favorite models of the electromagnetic theory of SERS) and also not on top of adatoms but rather in pores or crevices which were shown to exist on such coldly deposited films. In ref. [3] these pores are envisioned as narrow crevices 10–30 Å wide and ≈150 Å deep. However, the direct implication of these experiments is only that the most Raman active molecules are located as sites which are hidden to surface probes such as UPS and are also not accessible to the adsorbate in direct low-temperature (10–15 K) deposition. These sites are occupied at higher temperature (120 K for pyridine) due to surface migration of the adsorbate, leading to a substantial increase in the SERS signal.

While chemical interactions are expected to be stronger on some special sites such as kinks, steps or adatoms, it is hard to see their special role in such cavity sites. On the other hand, the local electromagnetic field intensity is strongly dependent on the local morphology and it is of interest to examine this intensity in different forms of cavity sites in comparison to flat surface and to protrusion sites. Recent calculations by Albano et al. [3] on surface plasmons in short period sinusoidal grating and by Wirgin and Lopez-Rios on electromagnetic resonances in a metallic surface with a periodic array of deep narrow one-dimensional grooves [5] indicate that the field in the deep channels of these periodic structures may indeed be very strong. It is unclear however to what extent the periodicity of the structure studied is essential for the existence of this behavior.

In this paper we examine two models of a "cavity site" in order to elucidate the role that may be played by such sites in SERS and other surface optical phe-

☆ Suported by the United States–Israel Binational Science Foundation, Jerusalem, Israel.

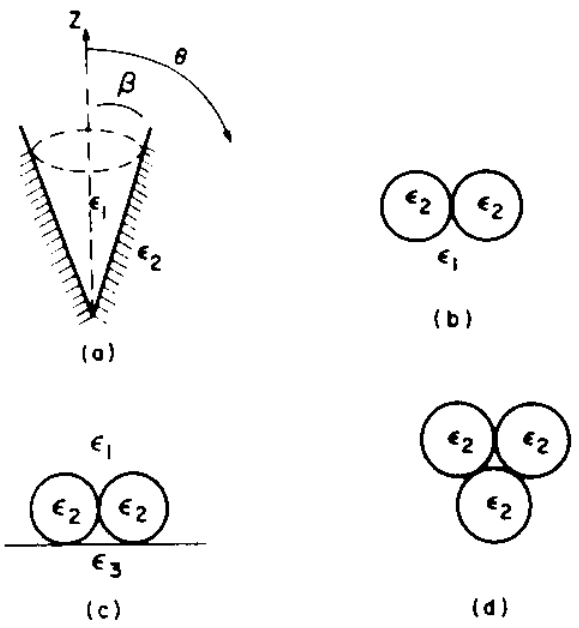

Fig. 1. Different configurations considered in the text. In (a) the cavity site is identified as the bottom of a conical wedge while in (b)–(d) it is taken to be a site which is partly enclosed by several grains.

nomena. The first model consists of a wedge (fig. 1a) which may be thought of as an approximation to the cavitey site suggested by Albano et al. [3]. The second model is a cluster of touching or nearly touching spheres (figs. 1b–1d) where the "cavities" are identified with regions partly enclosed by these spheres. In the calculations described below we invoke the electrostatic approximation implying that the electromagnetic field wavelength is much longer than the dimension of the structure studied. We find that the wedge structure generally leads to reduction of the field intensity relative to the incident field while in a cluster of spheres there are "hidden locations" where the field intensity may be considerably larger (by up to two orders of magnitude) than that in the outside regions which itself is strongly enhanced, near the dielectric resonance frequency, relative to the incident field.

2. The conical wedge

We consider the system displayed in fig. 1a where medium 2 is a metal and medium 1 is usually vacuum, air or water.

We seek solutions to the Laplace equation

$$\nabla^2 \Phi = 0 , \tag{1}$$

which satisfy the boundary conditions implied by fig. 1a and for simplicity we limit ourselves to solutions which are invariant to rotations about the Z axis. Inserting

$$\Phi = R(r)\, T(\theta) \tag{2}$$

into eq. (1) written in the form

$$\frac{1}{r^2}\frac{\partial}{\partial r}\left(r^2 \frac{\partial}{\partial r}\Phi\right) + \frac{1}{r^2 \sin\theta}\frac{\partial}{\partial\theta}\left(\sin\theta \frac{\partial}{\partial\theta}\Phi\right) = 0 . \tag{3}$$

The equation becomes separable. The equation for R is solved by

$$R = r^{\nu} \quad (r \geqslant 0) \tag{4}$$

and the corresponding equation for T is the Legendre equation

$$\frac{\mathrm{d}}{\mathrm{d}x}\left((1 - x^2)\frac{\mathrm{d}T}{\mathrm{d}x}\right) + \nu(\nu + 1)\, T = 0 , \tag{5}$$

where

$$X = \cos\theta . \tag{6}$$

The solution of eq. (5) is

$$T(x) = F(\nu + 1, -\nu, 1, \eta), \tag{7}$$

with

$$\eta = \tfrac{1}{2}(1 - |x|), \tag{8}$$

where $F(a, b, c, z)$ is the hypergeometric function. Denoting

$$\gamma \equiv \cos\beta , \tag{9}$$

the solutions of (1) take the form

$$\Phi = r^{\nu} F(\nu + 1, -\nu, 1, \tfrac{1}{2}(1 - x)), \quad \text{for } \gamma < x < 1 ;$$

$$= C r^{\nu} F(\nu + 1, -\nu, 1, \tfrac{1}{2}(1 + x)), \quad \text{for } -1 < x < \gamma. \tag{10}$$

Continuity of Φ near $\theta = \beta$ requires that

$$C = F(\nu + 1, -\nu, 1, \tfrac{1}{2}(1 - \gamma))/F(\nu + 1, -\nu, 1, \tfrac{1}{2}(1 + \gamma)), \tag{11}$$

while continuity of the θ component of the displacement field near $\theta = \beta$

$$[\mathrm{d}F(\nu + 1, -\nu, 1, \tfrac{1}{2}(1 - x))/\mathrm{d}x]_{x=\gamma}$$

$$= \epsilon C [\mathrm{d}F(\nu + 1, -\nu, 1, \tfrac{1}{2}(1 + x))/\mathrm{d}x]_{x=\gamma} \tag{12}$$

(where $\epsilon = \epsilon_2/\epsilon_1$) leads to

$$\epsilon = \frac{F(\nu+1,-\nu,1,\frac{1}{2}(1+\gamma))F(\nu+2,1-\nu,2,\frac{1}{2}(1-\gamma))}{F(\nu+1,-\nu,1,\frac{1}{2}(1-\gamma))F(\nu+2,1-\nu,2,\frac{1}{2}(1+\gamma))}, \quad (13)$$

where we have used the relation

$$\mathrm{d}F(a,b,c,z)/\mathrm{d}z = (ab/c)F(a+1,b+1,c+1,z). \quad (14)$$

Eq. (13) may now be used to examine the behavior of the electric field as a function of the distance from the wedge bottom. More specifically we look for values of the dielectric function ϵ which can sustain solutions with $0 \leqslant \nu < 1$. Such solutions correspond to a divergence of the field at the wedge bottom, similar to that obtained at the tip of a protruding cone.

In fig. 2 we show ν obtained from (13) as a function of ϵ for different values of γ. We see that for $\gamma > 0$ (conical pore) the range of real ϵ which corresponds to a diverging field at the bottom does not overlap the dielectric function of silver (Re $\epsilon < -1$ for frequencies in the visible range). This is in contrast to the conical protrusion ($\gamma < 0$) where conditions for large field near the tip are easily satisfied by the bulk dielectric functions of many metals. We conclude that the geometry of fig. 1a cannot explain the results of the experiments discussed above.

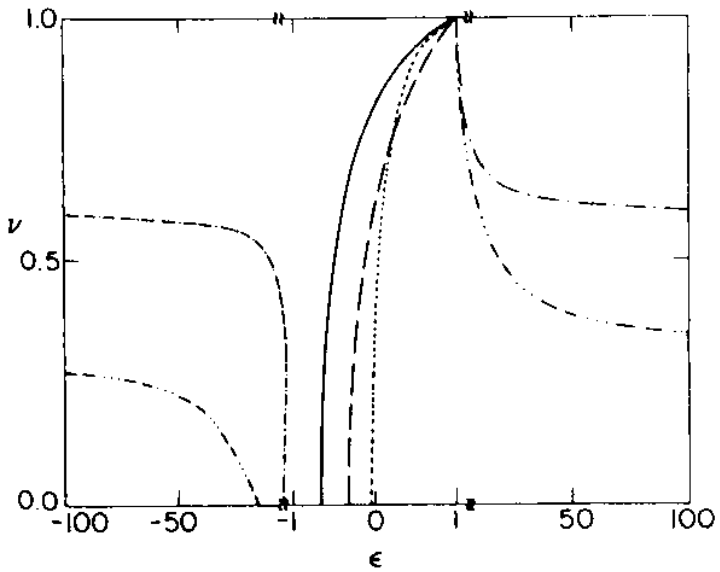

Fig. 2. The radical exponent ν (eq. (4)) as a function of the (real) dielectric constant ϵ for different values of $\gamma = \cos\beta$ (β, the conical wedge angle; $\gamma < 0$ corresponds to a conical protrusion). The lines corresponding to conical pores: $\gamma = 0.2$ (——), $\gamma = 0.5$ (– – –) and $\gamma = 0.9$ (...) show that values of ϵ that can support ν in the range 0–1 are confined to the range $-1 < \epsilon < 1$. Only for conical protrusions: $\gamma = -0.5$ (–·–·–) and $\gamma = 0.9$ (——···——) does $\epsilon < -1$ correspond to $0 \leqslant \nu < 1$.

3. Cavity sites in cluster of spheres

In order to study the local fields in structures like those displayed in figs. 1b–1d we use the formalism presented by Liver, Nitzan and Freed [6] (based on Bergman's theory of electrostatic resonances in composite dielectric systems) [7]. For a system of $N-1$ grains characterized by dielectric functions $\epsilon_1(\omega)$, $\epsilon_2(\omega)...\epsilon_{N-1}(\omega)$ imbedded in an infinite medium with dielectric function $\epsilon_N(\omega)$ and subjected to the influence of some charge density $\rho(r)$ the potential $\psi(r)$ at any point r is obtained in the form

$$\psi(r) = \epsilon_N^{-1}\psi_\rho(r) + \sum_{a=1}^{N-1} u_a \sum_\alpha C_{a\alpha}\psi_{a\alpha}(r), \quad (15)$$

where

$$u_a = 1 - \epsilon_a/\epsilon_N, \quad (16)$$

$$\psi_\rho(r) = 4\pi \int \mathrm{d}^3r'\, G(r|r')\,\rho(r), \quad (17)$$

$$G(r|r') = 1/4\pi(r-r'). \quad (18)$$

$\psi_{a\alpha}(r)$ are the eigenfunctions of the operator $\hat{G}_a$ defined by

$$\hat{G}_a\,\psi(r) = \int \mathrm{d}^3r'\,\theta_a(r')\,\nabla' G(r|r')\cdot\nabla'\psi(r'), \quad (19)$$

where θ_a is a step function which vanishes outside grain a and is equal to 1 inside it. Thus

$$\hat{G}_a\psi_{a\alpha} = s_{a\alpha}\psi_{a\alpha}. \quad (20)$$

For a spherical grain of radius r_a the index α represents the pair of integers (l,m) ($l = 1,2\ldots; m = -l,\ldots l$) and

$$\psi_{alm}(r) = (lr_a^{2l+1})^{-1/2}\, r^l\, Y_{lm}(\Omega), \qquad r \leqslant r_a;$$
$$= (lr_a^{2l+1})^{-1/2}\,(r_a^{2l+1}/r^{l+1})Y_{lm}(\Omega), \qquad r \geqslant r_a; \quad (21)$$

$$s_{alm} = l/(2l+1)\,. \tag{22}$$

Finally the expansion coeffieients $C_{a\alpha}$ are given by

$$C = \epsilon_N^{-1}\,(\mathbf{I} - \mathbf{Q})^{-1}\,D\,, \tag{23}$$

where C is the vector of $C_{a\alpha}$ coefficients, $\mathbf{Q}$ is a matrix whose elements are defined by

$$Q_{a\alpha;b\beta} = u_b\, s_{b\beta} \int \mathrm{d}^3 r\, \theta_a(r)\, \nabla \psi^*_{a\alpha}(r) \cdot \nabla \psi_{b\beta}(r) \tag{24}$$

and the elements of the vector D are given by

$$D_{a\alpha} = \int \mathrm{d}^3 r\, \theta_a(r)\, \nabla \psi^*_{a\alpha}(r) \cdot \nabla \psi_\rho(r)\,. \tag{25}$$

Explicit expressions for $Q_{alm;bl'm'}$ and D_{alm} for spherical grains are provided in ref. [6]. Given these we evaluate $C_{a\alpha}$ from eq. (23) by truncating the infinite-order multipole expansion at any desired order. The potential (or its spatial derivative – the local field) at any point r in the system is obtained from (15) using truncation at the same order. The convergence of this truncation procedure is discussed in ref. [6]. In the present work we are interested in the response of the system to a homogeneous incident field (representing an electromagnetic field whose wavelength largely exceeds the dimension of our system). This is simply achieved by putting the charge distribution (taken to be a point charge or a point dipole) very far from the system. We then calculate enhancement ratios such as

$$\eta_i(r) = |\nabla_i \psi(r)|^2 / |\nabla_i \psi_\rho(r)|^2 \quad (i = x, y, z)\,. \tag{26}$$

In the calculations reported below we use spherical silver particles for which we use the bulk dielectric function of silver [8]. Simple corrections to the dielectric function which take finite size effects into account may be introduced but do not change the conclusions reached here.

Fig. 3 displays the enhancement ratio η_x as a function of light frequency ω for a system of two identical spheres (x is the direction of both the incident field and the line connecting the sphere centers). The distance between the sphere centers is 2.2 in units of the sphere radius. (These units are used in all following discussion.) Here and in the following calculations we truncate the multipole expansion after $l = 8$. Convergence at this l was tested and found to be very good. We compare the enhancement ratios at two locations (denoted a and b in the inset): one at exactly

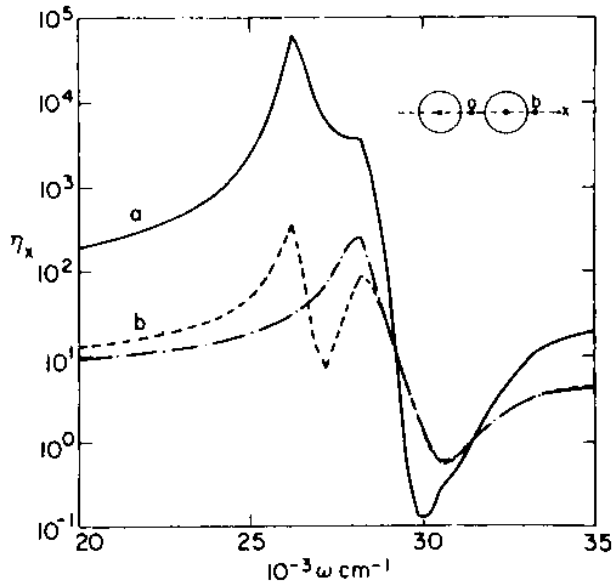

Fig. 3. The enhancement ratio η_x as a function of the incident frequency at two locations (denoted by a (full line) and b (dashed line) in the inset) near a cluster of two silver spheres. The dash-dotted line gives similar results for a molecule in a similar configuration near a single silver sphere.

the midpoint on the line connecting the two spheres (essentially a cavity site) and the other on the same bispherical axis, on the outer side at distance 0.1 from the sphere surface. In fig. 4 we present similar results for a system of four identical spheres. The sphere cen-

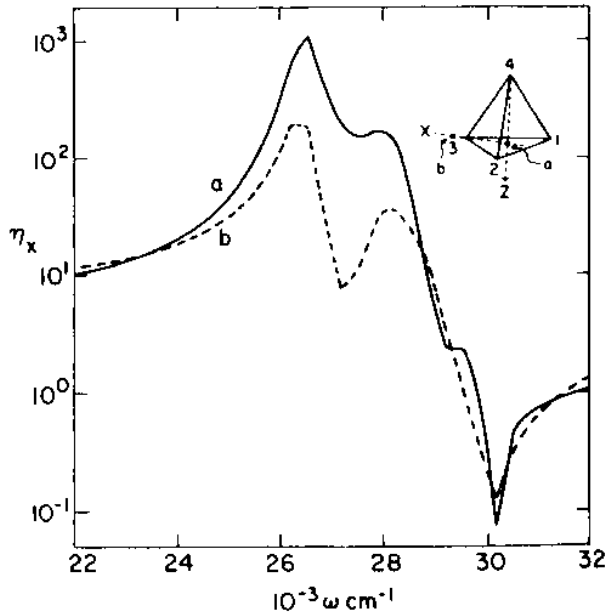

Fig. 4. The enhancement ratio η_x as a function of the incident frequency at two locations (marked a and b in the inset) near a cluster of four silver spheres.

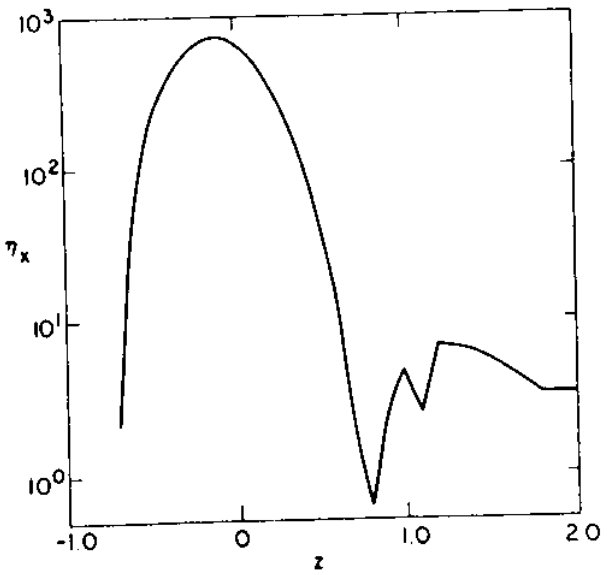

Fig. 5. The enhancement ratio η_x in the configuration of fig. 4 as a function of the distance z along the line connecting the center of sphere 4 with the center of the 123 face.

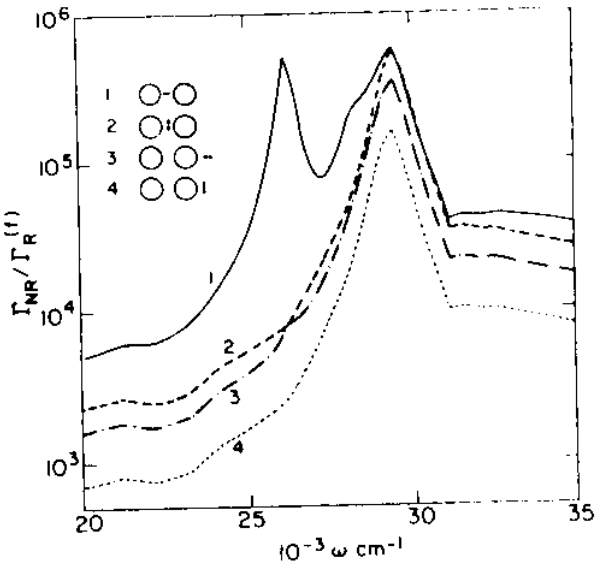

Fig. 6. Non-radiative decay rate of a molecule as a function of the molecular frequency at different locations and orientations near a two-silver-sphere cluster. The different configurations are shown in the inset with the double arrows denoting the position and orientation of the point polarizable particle representing the molecule. The sphere radii are 100 A and the distance between their centers is 220 A. The molecule is located at a distance of 10 A from the surface of the nearest sphere along the line joining the sphere centers.

ters lie on the corners of a tetrahedron (see inset) of side length 2.2. η_x is calculated at the center (a) of the 123 face and at a point (b) lying outside the tetrahedron at a distance of 1.25 from the center of sphere 3 along the line connecting the center of sphere 3 with the center of the 123 face. (This is also the distance of point a from the sphere centers.) In fig. 5 the enhancement ratio η_x in the configuration of fig. 4 is plotted as a function of distance along the line connecting the center of sphere 4 to the center of the 123 plane (z axis in the inset of fig. 4). In this figure the origin is taken as the center of the 123 face (point a of the inset of fig. 4) and the center of sphere 4 lies in the $-z$ direction.

It is seen that for these clustered sphere configurations the local field is substantially higher in the space confined between the spheres which is largely hidden to normal surface probes and thus constitutes a cavity site. Such an effect has already been reported for the two-sphere systems by Aravind, Nitzan and Metiu [9]. This is in contrast to the conical wedge like geometry discussed in section 2. It should be stressed that the enhancement ratio (26) is defined for the field intensity and that the enhancement of the Raman scattering signal will be roughly the square of this quantity. The electromagnetic cavity site enhancement is thus seen to be related to the plasmon resonance of the clustered grain system where the field is seen to be more focussed and thus stronger in regions of near contact between these grains.

For many applications which involve resonance excitation of the molecule (e.g. photochemistry [10]) the net surface effect on the molecular response to an incident radiation results from the balance between the local field enhancement and the surface induced damping of the molecular excitation. For this reason it is of interest to compare also this damping rate at different sites. Results of such calculations (based on the procedure developed by Liver et al. [6]) are shown in fig. 6. By comparing these results to those of fig. 3 it is seen that even though both the local field and the damping rate are larger between the spheres than on the outside, the enhancement of the local field between the spheres is considerably stronger than that of the damping rate. Cavity sites are therefore expected to be favorable also for enhancement of resonance optical processes such as fluorescence and photochemistry.

4. Conclusion

The stronger SERS signal suggested by recent experiments to be associated with cavity sites in coldly evaporated porous silver films is consistent with the stronger local field enhancement obtained in the present calculation for cavities enclosed by several touching or nearly touching small spheres. No such enhancement is obtained for a wedge like geometry which is adversely affected by an inverse lightning rod effect. Such cavity sites were shown by the present calculation to give stronger enhancement of resonance optical phenomena.

Acknowledgement

We would like to thank Drs. Chuang and Seki for communicating their experimental results prior to publication.

References

[1] H. Metiu and P. Das, Electromagnetic Theory of Surface Enhanced Spectroscopy, to be published; M. Kerker, An Electromagnetic Model for SERS on Metal Colloids, Accounts Chem. Res., to be published; J. Gersten and A. Nitzan, in: Surface enhanced Raman scattering, eds. R.K. Chang and T.E. Furtak (Plenum Press, New York, 1981).

[2] A. Otto, in: Light scattering in solids, Vol. 4, eds. M. Cardona and G. Guntherodt (Springer, Berlin, 1983).

[3] E.V. Albano, S. Daiser, G. Ertl, R. Miranda, K. Wandelt and N. Garcia, Phys. Rev. Letters 51 (1983) 2314.

[4] H. Seki and T.J. Chuang, Chem. Phys. Letters 100 (1983) 393.

[5] A. Wirgin and T. Lopez-Rios, Opt. Commun. 48 (1984) 416;
T. Lopez-Rios and A. Wirgin, Role of Waveguide and Surface Plasmon Resonances in SERS at Coldly Evaporated Silver Films, to be published.

[6] N. Liver, A. Nitzan and K.F. Freed, Radiative and Non-Radiative Decay Rates of Molecules Adsorbed on Clusters of Small Dielectric Particles, to be published.

[7] D.J. Bergman, in: Lecture notes in physics, Vol. 154, eds. R. Burridge, S. Childress and G. Papanicolaou (Springer, Berlin, 1982) p. 10.

[8] P.B. Johnson and R.W. Christy, Phys. Rev. B6 (1972) 4370.

[9] P.K. Aravind, A. Nitzan and H. Metiu, Surface Sci. 110 (1981) 189.

[10] A Nitzan and L.E. Brus, J. Chem Phys. 75 (1981) 2205.